Research Article | Vol. 29, No. 26 / 20 Dec 2021 / Optics Express 43226

Optics EXPRESS

4-domain twisted liquid crystal micropolarizer array for visible linear polarization imaging

SHIYUAN ZHANG,[1,2] CHANG LIU,[3] ZIJUN SUN,[1,2] QUANQUAN MU,[1,2,*] JUAN CAMPOS,[4] HUA LIU,[3] XINGYUN ZHANG,[1] DAYU LI,[1,2] AND QIDONG WANG[1]

[1] *Changchun Institute of Optics, Fine Mechanics and Physics, Chinese Academy of Sciences, Changchun 130033, China*
[2] *Center of Material Science and Optoelectronics Engineering, University of Chinese Academy of Sciences, Beijing 100049, China*
[3] *School of Physics, Northeast Normal University, Changchun 130033, China*
[4] *Grup d'Òptica, Physics Department, Universitat Autònoma de Barcelona, Bellaterra 08193, Spain*
[*] *muquanquan@ciomp.ac.cn*

Abstract: In this paper, a 4-domain twisted liquid crystal micropolarizer (twisted-LCMP) array was designed and fabricated enabling linear polarization imaging in the visible band. It contains a pixelized twisted-LC layer and a polarizer. The optimized twist angles were designed as ±22.5° and ±67.5° for best extinction ratio. A large birefringence LC material was used to fulfill the Mauguin condition in a wider visible band. Using a digital micromirror device (DMD) lithography system, the twisted-LCMP array was fabricated precisely using the photoalignment technique. It exhibited excellent optical performance, which could meet the requirements for polarization imaging. The measurement error for degree of linear polarization (DoLP) and angle of polarization (AoP) were less than 1.15% and 0.65°. The proposed twisted-LCMP array has great potential to be integrated directly into a camera for real-time linear polarization imaging.

1. Introduction

Polarization imaging, one of the most important optical imaging methods, provides variety of information about targets compared with conventional imaging methods. Polarization imaging offers numerous benefits, not only detecting geometry and surface, but measuring physical properties which couldn't be recognized by conventional imaging. It has important application potential in remote sensing [1,2], interferometry [3,4] and biomedical physics [5,6], and has been widely studied by scholars around the world.

There are many kinds of imaging polarimeters could be used for polarization imaging [7]: Division of Time Polarimeter (DoTP), Division of Amplitude Polarimeter (DoAmP), Division of Aperture Polarimeter (DoAP), and Division of Focal-plane Polarimeter (DoFP). Due to the use of a micropolarizer array as its core component, the DoFP type is most attractive for its compact structure, robust and real-time dynamic acquisition [7–9].

Many types of micropolarizer arrays have been studied and used, such as micro-wire-grid polarizers (MWGP) [9–10], patterned polyvinyl-alcohol (PVA) polarizer [11–12] and liquid crystal micropolarizer (LCMP) array [13–19]. An MWGP array is usually prepared by electron beam lithography (EBL) and inductively coupled plasma-reactive ion etching (ICP-RIE). This requires complex lithography and chemical processing to achieve nanoscale accuracy. For example, the MWGP proposed in Ref. [10] has a grating period of 140 nm and duty cycle of 0.5. The process is complex and costly, and the uniformity is difficult to ensure. While a PVA micropolarizer array is usually prepared by etching multilayer PVA polarizers. Therefore, the overall thickness is large (more than 10 μm). This will aggravate the cross crosstalk between adjacent pixels. And it also requires high-precision etching and alignment [11]. LCMP array,

#446128 https://doi.org/10.1364/OE.446128
Journal © 2021 Received 18 Oct 2021; revised 25 Nov 2021; accepted 25 Nov 2021; published 10 Dec 2021

by contrast, has the advantages of simple structure, stable performance and cost-effective. The orientation of LC molecules can be controlled by the photoalignment methods in micron-scale [20]. Thus, it does not require high-precision exposure etching and complex chemical processes.

For linear polarization imaging, the LCMP can be categorized as either a dichroic absorption LCMP or a polarization rotator LCMP. A dichroic absorption LCMP with guest dichroic dye doped in host LC material could form a LC polymer (LCP) guest-host device [15–17,19]. The dichroic dye molecules are cooperatively aligned with the LC director. It works similarly to a patterned polyvinyl-alcohol (PVA) micropolarizer array, but thinner. For host-guest LCMP, due to the limitation of dichroic dyes, its extinction ratio is usually only about 10 to 100, and only covers a narrow band in visible spectrum. A polarization rotator LCMP [13,14] consists of a pixelated twisted-LC layer, which serves as a polarization rotator, and a linear polarizer. The linear polarizer mainly determines the extinction ratio and transmittance of the LCMP array. The polarization rotator LCMP array can be designed to achieve high extinction ratios (greater than 1000) and cover different bands from visible to infrared. Reference [13] proposed an LCMP generated 2 polarization analyzers (0° and 90° micropolarizers). Only the first two components of the Stokes vectors can be obtained, which is not enough for linear polarization imaging.

Based on the structure of polarization rotator LCMP, a 4-domain twisted-LC micropolarizer (twisted-LCMP) array with high extinction ratio in visible light band is introduced in this paper. The design, preparation and imaging performance of the device are studied. A digital micromirror device (DMD) lithography system was used to fabricate the twisted-LCMP array, which avoided the alignment error caused by multiple masking exposures. The first three components of the Stokes vector were used to estimate the incident polarization state. The results indicate that the polarimeter system based on twisted-LCMP has high measurement accuracy and can meet the requirements of polarization imaging.

2. Twisted-LCMP array design

The twisted-LCMP array consists of a pixelated twisted LC layer and a uniform linear polarizer, shown in Fig. 1. The LC layer modulates the polarized light in different directions, and the linear polarizer analyzes the final polarization state. Each unit (called a superpixel) contains 4 sub-pixels with different twist angles. They rotate the polarization direction of incident linear polarized light with four different directions into the same direction parallel with the linear polarizer. On the bottom side, the LC molecules have a constant orientation parallel to the polarization direction of linear polarizer. The pixelized orientation of LC molecules was achieved by the photo alignment technique on the top side. To get an excellent rotation performance, every sub-pixel should meet the Mauguin condition [21] under the same thickness.

$$u = \frac{\mathit{\Gamma}}{2\Phi} = \frac{\pi}{\Phi}\frac{\mathit{\Delta} n(\lambda)d}{\lambda} \gg 1;\ \text{where}\ \mathit{\Gamma} = \frac{2\pi}{\lambda}\mathit{\Delta} n(\lambda)d. \tag{1}$$

Where u is the Mauguin parameter, $\mathit{\Gamma}$, $\mathit{\Phi}$, and d are the phase retardation, twist angle and the thickness of LC layer, respectively. $\Delta n(\lambda)$ is the birefringence of the LC material and λ is the wavelength.

Equation (1) shows that we need to reduce the twist angle $\mathit{\Phi}$ and increase Δnd to satisfy the Mauguin condition. Next, we analyze how we face these requirements.

For linear polarization detection with high signal-to-noise ratio, the optimal configuration is to detect four different linear polarization measurements uniformly distributed from 0° and 180°

Optics EXPRESS

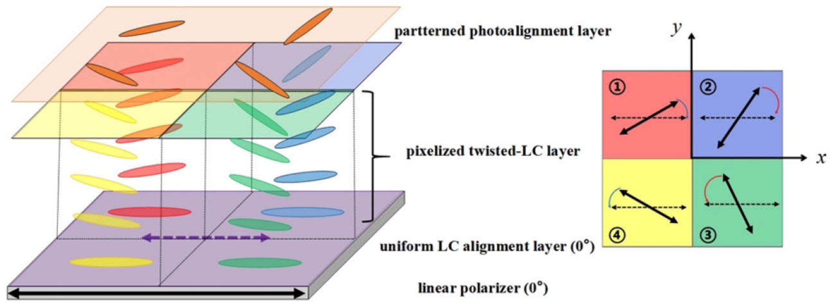

Fig. 1. Schematic diagram of a superpixel of the proposed twisted-LCMP array.

[22]. Thus, the LC orientation interval between each sub-pixel should be 45°, shown in Eq. (2).

$$\begin{cases} 0^\circ \le \Phi_1 \le 45^\circ \\ \Phi_2 - \Phi_1 = 45^\circ, (45^\circ \le \Phi_2 \le 90^\circ); \\ |\Phi_3| - \Phi_2 = 45^\circ, (-90^\circ \le \Phi_3 \le -45^\circ); \\ |\Phi_3| - |\Phi_4| = 45^\circ, (-45^\circ \le \Phi_4 \le 0^\circ). \end{cases} \tag{2}$$

In such a condition, 22.5°, 67.5°, −67.5° and −22.5° is the combination of the twist angles with minimum absolute values that can be achieved. For other orientations, there will always be a twist angle greater than 67.5° ($|\Phi| > 67.5\,^\circ$) in the superpixel, as shown in Fig. 2.

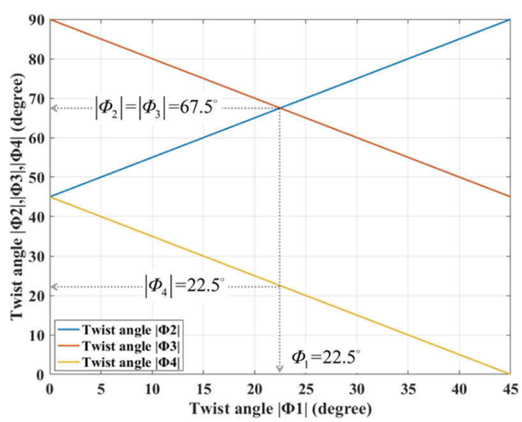

Fig. 2. Relationship between the four twist angles Φ. When Φ_1 takes 22.5°, for $|\Phi_2| = |\Phi_3| = 67.5^\circ$ and $|\Phi_4| = 22.5^\circ$. This is the twist angle combination with minimum absolute values that can be achieved.

We use a LC material (LC-4k) with large birefringence ($\Delta n_{\text{LC-4K}} = 0.404$, @ 589 nm) synthetized in our laboratory [23,24]. It is a mixture of several compounds with fluorinated (F) and isothiocyanato (NCS) groups, and shows a good photo and thermal stabilities [25]. LC-4k has a wide range of LC phase temperature (melting point T_m and clear point is about −29.32 °C and 108.91 °C, respectively). Its birefringence Δn (tested at 25 °C) can be expressed by the extended Cauchy Equation:

$$\Delta n_{LC-4k}(\lambda) = n_e(\lambda) - n_o(\lambda) = 0.275 + \frac{44790}{\lambda^2} + \frac{0.1978}{\lambda^4}. \tag{3}$$

Optics EXPRESS

To better fulfill the Mauguin condition, the thickness of LC layer should be increased. But the increased thickness will aggravate the crosstalk between adjacent pixels. To get the best LC thickness, the relationship between the LC thickness and its polarization rotation efficiency is studied. The polarization efficiency PE [16] and extinction ratio EXR are used to evaluate the performance:

$$PE = \sqrt{\frac{T_{\parallel} - T_{\perp}}{T_{\parallel} + T_{\perp}}} \times 100\%, \; EXR = \frac{T_{\parallel}}{T_{\perp}} = \frac{1 + PE^2}{1 - PE^2}. \tag{4}$$

Where $T_{\parallel}$ and $T_{\perp}$ represent the transmittance of the twisted-LC polarizer when the polarization direction of incident beam is parallel or perpendicular to the LC director at the entrance plane, respectively, which can be derived from the Jones matrix [21]:

$$T_{\parallel} = 1 - \Phi^2 \frac{\sin^2 X}{X^2}, \; T_{\perp} = \Phi^2 \frac{\sin^2 X}{X^2}; \text{ with } X = \sqrt{\Phi^2 + \left(\frac{\Gamma}{2}\right)^2}. \tag{5}$$

To better describe the broadband characteristics of the device, the average polarization efficiency $\overline{PE}$ shown in Eq. (6), is used.

$$\overline{PE}(d) = \frac{1}{N}\left(\sum_{i=1}^{N} PE(\lambda_i, d)\right). \tag{6}$$

It is assumed that the light intensity is equal for the whole visible band (400-800 nm, N=401), the $\overline{PE}$ relationship for 22.5° and 67.5° twist angles is shown in Fig. 3(a). The results show that $\overline{PE}$ changes little when the thickness is greater than 4 µm for 22.5° twist angle. While for 67.5° twist angle, when the thickness is less than 6 µm, $\overline{PE}$ increases rapidly, and when the thickness is greater than 7 µm, $\overline{PE}$ changes little. For the 67.5° twist angle, there are two maxima of $\overline{PE}$ at the thickness of 4.3 µm and 6.6 µm. In Fig. 3(b), we show the bandwidth and the percentage of the whole 400 nm bandwidth that gives a PE higher than different values represented in different colors. As shown in Fig. 3(b), when the thickness is 6.6 µm, PE is higher than 0.99 ($EXR > 100$) in most (91.8%) wavelengths; and PE is higher than 0.998 ($EXR > 500$) in nearly half (47.1%) of the whole visible band.

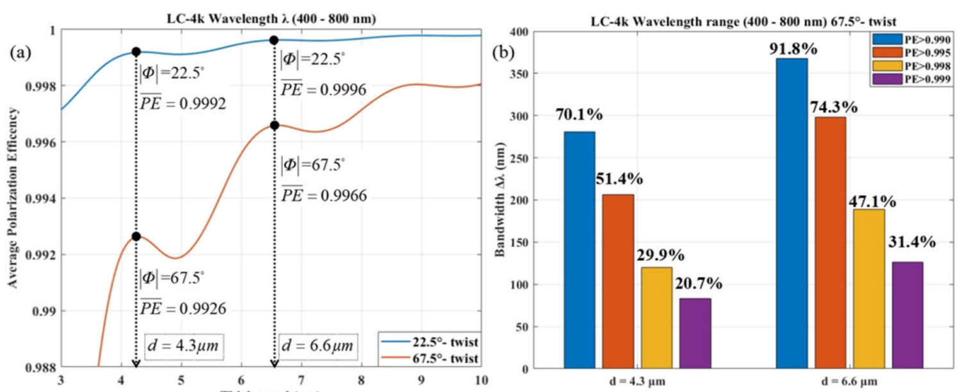

Fig. 3. (a) The relationship between the average polarization efficiency $\overline{PE}$ of the 22.5° and 67.5° twisted LC polarizer and the thickness d of the LC layer in the visible band (400-800 nm). (b) The 67.5° twist angle at the thickness of 4.3 µm and 6.6 µm was analyzed. The polarization efficiency PE is greater than 0.990, 0.995, 0.998 and 0.999 band widths $\Delta\lambda$, respectively.

In summary, utilizing the large-birefringence LC material made in our laboratory, LC-4k, the optimized twisted-LCMP array was found to have the following parameters: twist angles $\Phi = \pm 22.5°$ and $\pm 67.5°$ for sub-pixels; the thickness $d = 6.6$ μm. The fabrication process and characterization of the twisted-LCMP array are described in the following section.

3. Twisted-LCMP array fabrication and characterization

The photo-rubbing mixed alignment technology was adopted in this paper to fabricate the twisted-LCMP array device, shown in Fig. 4(a). By rubbing the polyimide (PI) film along the edge of the bottom substrate, the LC molecules were aligned planarly along the horizontal direction (0°). Photoalignment was achieved by irradiating sulfonic azo-dye (SD1) layer with linearly polarized ultraviolet light (LPUV). The SD1 powder was dissolved in dimethylformamide (DMF) at a concentration of 0.5% (in weight). The solution was spin-coated at 3000 rpm for 30 s onto the substrates. Afterwards, the coated SD1 layer was annealed at 110 °C over 15 min for complete removal of DMF [26]. To avoid alignment defects, spacers cannot be sprayed directly onto the substrate. Hence, the two substrates were assembled together using sealant (NOA-68) mixed with spherical spacers (6.5 μm in diameter, 3% by weight) to keep the cell gap. By adjusting the width of the sealant and pressing pressure on the substrates, the thickness of the empty cell was formed with accuracy for 6.6 ± 0.1 μm.

After the empty cell was prepared, digital micromirror device (DMD) lithography system [27,28] was used to carry out the pixelated photoalignment for SD1 layer as shown in Fig. 4(b). Using a 405 nm LED light source, the pattern on the DMD was projected onto the SD1 layer through an objective. The rotatable polarizer P_1 was used to generate linear polarized light in different directions. The reflected beam from the imaging plane passed through the beam splitter and entered the CCD for fine focusing. The twist angle of each sub-pixel is a crucial factor for polarization measurement and imaging. The LC orientation interval between each sub-pixel should be 45° on the SD1 layer and the error of twist angles should be less than $\pm 1°$. Thus, it is important to calibration the direction of the P_1. This process is shown in Fig. 4(c). Due to the orientation of SD1 is perpendicular to the polarization direction of irradiated LPUV light [29], the direction of polarizer P_1 should be orthogonal to the rubbing direction, to give SD1 film initial orientation same as rubbing direction. The polarizer P_1 was fixed on a rotation stage with a high accuracy of about $\pm$ 820 μrad, ensuring 45° alignment intervals between each sub-pixel. The polarizer P_2 was fixed at 0° above P_1 on the mechanical structure of DMD system. Rotate P_1 by 360° and record the transmission intensity using a power meter. A sine curve fitting was achieved. The initial orientation of P_1 was fitted to be 124° with an uncertainty of $\pm 0.7°$. After P_1 was calibrated, P_2 was replaced with the empty LC cell along 0° with rubbing direction on PI substrate. The photoalignment process of SD1 layer is shown in Fig. 4(d). Rotate the polarizer P_1 to the corresponding angle and project the four mask images onto the SD1 layer respectively to form the pixelated orientation. For each mask image, the exposure dose is 5 J/cm^2 to achieve a strong azimuthal anchoring energy.

As shown in Fig. 4(e), LC-4k material was injected into the empty LC cell at 70 °C after photoalignment, and ergo epoxy adhesive was used as end-sealing. Then, a dichroic film polarizer (EXR > 100 for 400 - 500 nm, EXR > 1000 for 500 - 550 nm, EXR > 7000 for 550 - 680 nm) was manually pasted onto the outer surface of the bottom substrate using a protractor. The axis of the polarizer was consistent with the rubbing direction, and the orientation error is less than $\pm 0.5°$.

The sub-pixel size of the twisted-LCMP was determined by the DMD lithography system. This method does not need alignment masks, only the rotation of a polarizer and the display of a different mask in the micromirror device. The DMD used in this system (DLP7000UV, Texas Instruments Inc.) consists of 1024×768 micro-mirrors, with single pixel pitch of 13.68 μm. The pattern on the DMD can be de-magnified and projected onto the SD1 layer through an objective. For polarization measurement and imaging experiments, we used a 2x objective and combined

Optics EXPRESS

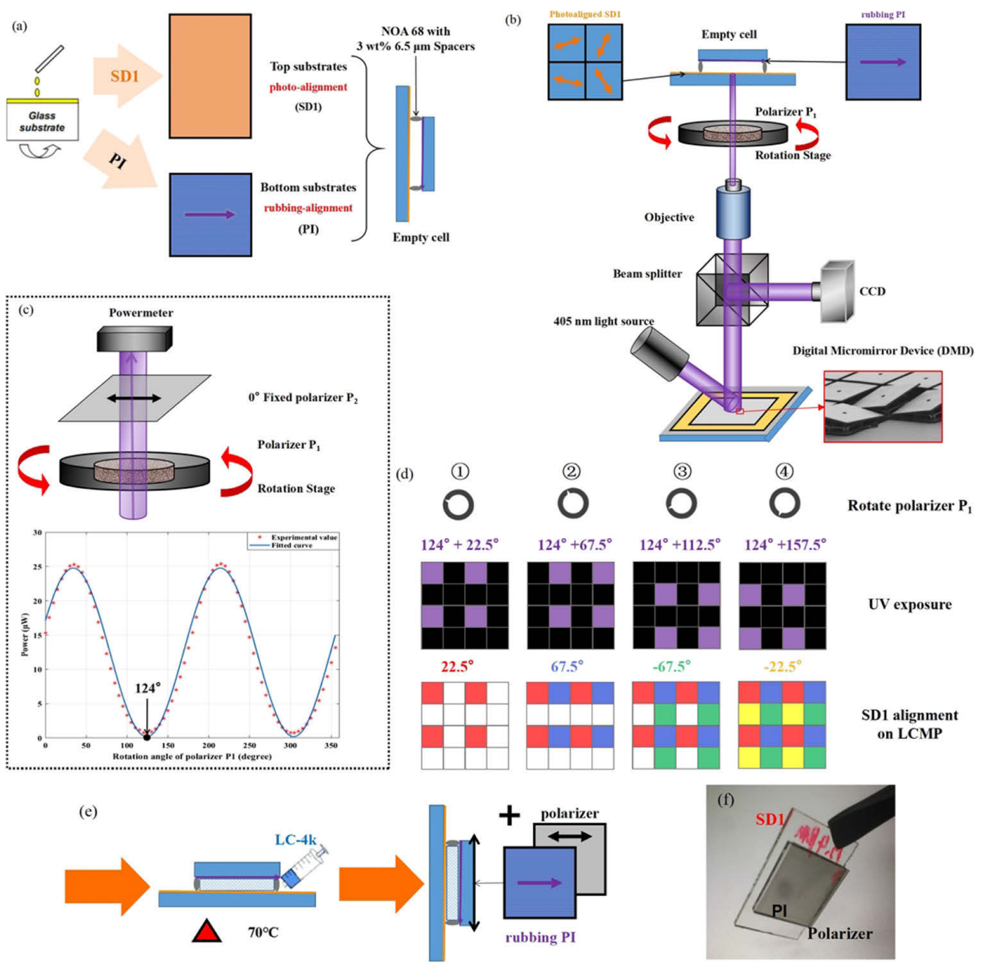

Fig. 4. Fabrication process of the proposed twisted-LCMP array. (a) Prepare an empty LC cell. (b) Schematic draw of the DMD lithography system. (c) Calibrate the initial orientation of polarizer P_1. (d) The photoalignment process of SD1 layer (e) Inject LC-4k into the empty cell and paste the film polarizer on the outer surface of the bottom substrate. (f) Photo of a twisted-LCMP array device.

13 × 13 DMD pixels into one unit for photoalignment exposure. Thus, the twisted-LCMP array with a sub-pixel pitch of 88.92 μm (13.68 μm / 2 × 13) was obtained. This resolution is only for principle test, it is not an indication of the resolution limit of the proposed twisted-LCMP fabrication technique. By using high-magnifying objectives and/or by combining less pixels on DMD, smaller pixel pitch could be achieved easily. The pattern of twisted-LCMP array was characterized using polarizing microscope. Figure 5 shows the sample's microphotographs examined by a linear polarizer. When the sample was illuminated by ± 22.5° and ± 67.5° linearly polarized light, the corresponding twisted-LCMPs showed bright state, and the whole device is uniform with few defects.

To measure the maximum polarized light transmittance and extinction ratio of the twisted-LCMP array, two single-twisted (22.5° and 67.5°-twisted) LC polarizers with size of 15 mm × 15 mm were prepared. The transmittance testing set up is shown in Fig. 6(a). A deuterium halogen tungsten light source (DH-2000-BAL) and a linearly polarized plate were used to generate 0°

Optics EXPRESS

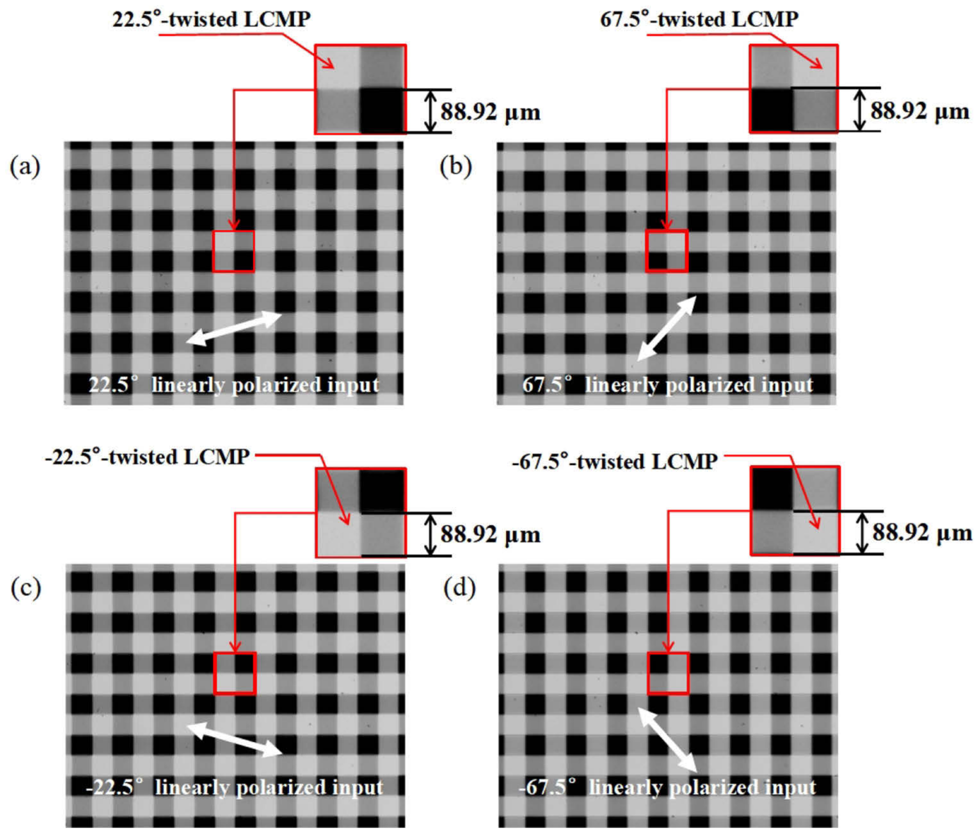

Fig. 5. Microphotographs of a fabricated twisted-LCMP array show the four twisted-LC polarizers in one superpixel (red square). The sample was illuminated with linearly polarized input light oriented at: (a) 22.5°; (b) 67.5°; (c) −22.5° and (d) −67.5°;

linearly polarized incident light. The single-twisted LC polarizer sample was fixed on the high precision stepper motor rotation stage (K10CR1, from Thorlabs Inc.), and the rotation stage was controlled by computer to rotate 180° continuously during the test. At the same time, a fiber spectrometer (USB4000, from Ocean Optics Inc.) was used to record the spectral transmittance at 5° intervals. The transmittance of the samples under blue (450 nm), green (550 nm) and red (650 nm) light are shown in Fig. 6(b) - (c). For the 22.5° and 67.5°-twisted LC polarizer, it shows that Malus law can be well satisfied. And the twisted-LC layer has little effect on the original maximum polarization transmittance (about 75%) of the film polarizer.

Further, we replaced the light source and detector with a He-Ne laser (@632.8 nm) and an optical power meter (PM100, from Thorlabs) to accurately measure the extinction ratios of the 22.5° and 67.5°-twisted LC polarizer. The extinction ratio calculation (*EXR*) can be expressed as:

$$EXR = \frac{P_{\parallel} - P_0}{P_{\perp} - P_0}. \tag{7}$$

where, $P_{\parallel}$ and $P_{\perp}$ are the transmitted light power when the incident linearly polarized light is parallel or perpendicular to the LC director at the entrance plane. P_0 is the average power of background in the darkroom. The test results are summarized in the Table 1.

At 632.8nm wavelength, the extinction ratio of the film polarizer is 8067. And the polarization efficiency *PE* decreases with the increase of the twist angle, so the *EXR* of the 22.5°-twist LC polarizer is relatively larger, which is consistent with our previous conclusion. For a 6.6 μm LC

Optics EXPRESS

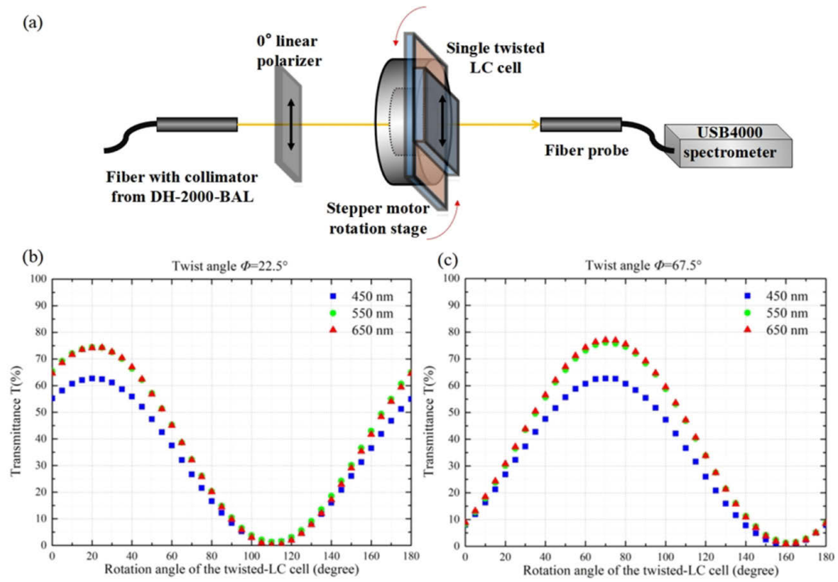

Fig. 6. (a) Transmittance test set up. The transmittance of (b) 22.5°- and (c) 67.5°-twisted LC polarizer at 450 nm, 550 nm and 650 nm conformed to Malus law.

Table 1. Extinction ratios of the dichroic film polarizer and two different twisted-LCMPs at 632.8 nm

	$P_{\parallel}$ (μW)	$P_{\perp}$ (μW)	P_0 (μW)	*EXR*
Dichroic film polarizer	960	0.130	0.011	8067
22.5°-twisted LC polarizer	855	0.147	0.011	6286
67.5°-twisted LC polarizer	756	0.522	0.011	1479

layer, the theoretical *EXR* of 22.5° and 67.5°-twist LC polarizers calculated by Jones matrix are 7316 and 2838 (@ 632.8 nm), respectively. The test values (6286 and 1479) are slightly lower which can be attributed to small deviation in fabrication.

4. Polarization measurement and imaging experiments

4.1. Establishment and calibration of polarimeter system

In order to verify the performance of the proposed twisted-LCMP, series of polarization measurement and imaging experiments were carried out. The optical set up is shown in Fig. 7. A monochromatic collimating beam was generated using a white LED, a collimating lens and a bandpass filter with full width at half maxima (FWHM) of 10 nm. The central wavelengths of the filters used in the experiment were 488 nm, 546 nm and 633 nm, respectively. Series of incident light with different polarization states were obtained by rotating linear polarizer and achromatic λ/4 waveplate (AQWP10M-580, Thorlabs). A monochrome COMS camera (DCC1545M, Thorlabs) with pixel size of 5.2 μm and resolution of 1280*1024 (8-bit grayscale) was used to capture the image. Using a double telecentric lens (F/12) as a relay lens, the twisted-LCMP array could be imaged on the focal plane of the camera forming a polarimeter system.

Firstly, the twisted-LCMP should be aligned with CMOS array. It has been reported that [30] alignment deviation along x and y needs to be controlled within 10% of the size of the micropolarizer pixels to maintain good performance of the DoFP. Each sub-pixel size of the twisted-LCMP array is 88.92 μm, roughly equivalent to 17 CMOS pixels (88.4 μm). Therefore,

Optics EXPRESS

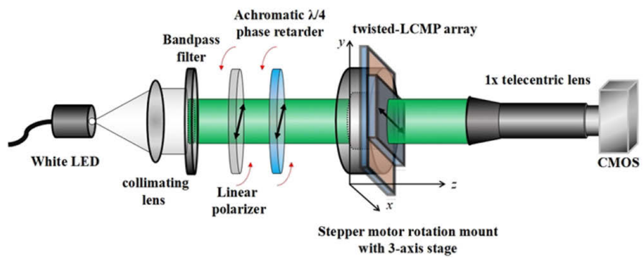

Fig. 7. Schematic diagram of the polarimeter set up.

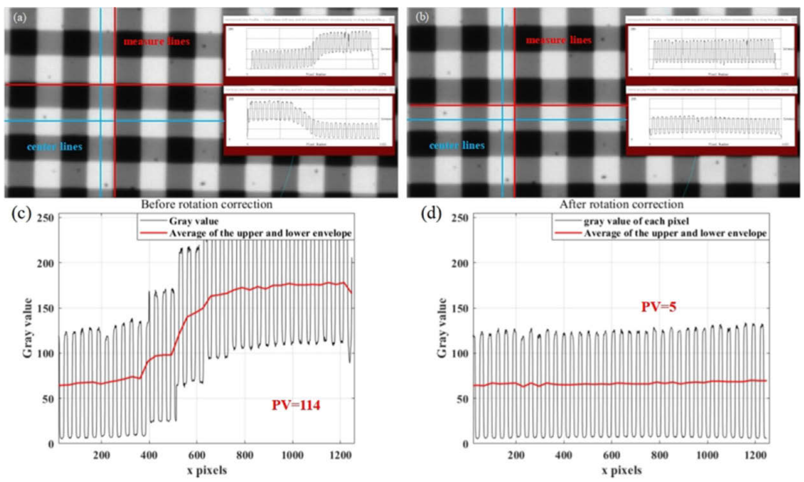

Fig. 8. The rotation error was corrected by measuring the change of the line profile at the edge of LCMP pixels (red measurement line). The average PV of upper and lower envelopes should tend to be 0. (a), (c) Before correction, PV=114; (b), (d) After correction, PV=5.

alignment along x and y is not required, while the rotation error needs to be controlled within 0.2° to meet the deviation less than 10% of sub-pixels on the edge. During alignment, the CMOS sensor was illuminated with 22.5° polarized light and the LCMP array can be clearly imaged on the sensor through the relay lens by adjusting the 3-axis stage. Then, the stepper motor rotation mount was fine-tuned with step of 0.05° to correct the rotation error until the horizontal and vertical line profile on the edge of the LCMP pixels became uniformly. That is, the average PV of upper and lower envelopes tended to be 0. The comparison before and after rotation correction are shown in Fig. 8(a)-(b). The change of horizontal line profile at the edge of LCMP pixels are shown in Fig. 8(c)-(d). The PV drops from 114 to 5 after correction.

As shown in Fig. 9, correlation algorithm was used to calculate the central coordinates (x, y) of each 22.5°-twisted sub-pixel corresponding to the CMOS array. Then the central coordinates of the other three neighbor sub-pixels $(x + 17, y)$, $(x, y + 17)$ and $(x + 17, y + 17)$ were determined. These four sub-pixels composed one superpixel (X, Y), and there were 29×35 superpixels in the scene. The average gray value within the range of 9×9 in center of each LCMP pixel was extracted as the measured intensity, $\boldsymbol{S_{out,0}}$.

The conventional polarimetric data reduction matrix method [18] is adopted for the calibration at each measured wavelength used in this paper. The device is illuminated with a series of n uniform linearly polarized state beams generated by rotating a polarizer. We will use the first three components of the Stokes vector $(S^k) = (S_0^k, S_1^k, S_2^k)^T$, $k = 1, \ldots, n$. To each sub-pixel $m = 1,$

Optics EXPRESS

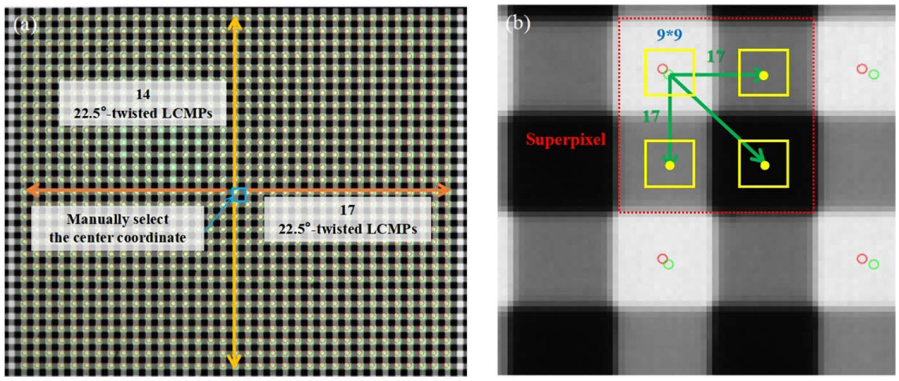

Fig. 9. A correlation algorithm was used to determine the position of each pixel. (a) There are 29×35 superpixels in total. First, manually select the center coordinate (in the blue square) and calculate the initial position of the 22.5°-twisted sub-pixel (red circles). Then, their center coordinates (green circles) calculated using correlation algorithm. (b) shows a partial enlargement of the image. The centers of the other three adjacent sub-pixels (yellow points) were then determined. Extract the average gray value in the center of each sub-pixel within the range of 9×9 (yellow squares) as the measured intensity value.

2, 3, 4 will have an associated analyzer. Then the measured calibration intensities can be written as:

$$\begin{pmatrix} I_{1,1} & \cdots & I_{1,n} \\ I_{2,1} & \cdots & I_{2,n} \\ I_{3,1} & \cdots & I_{3,n} \\ I_{4,1} & \cdots & I_{4,n} \end{pmatrix} = \begin{pmatrix} A_0^1 & A_1^1 & A_2^1 \\ A_0^2 & A_1^2 & A_2^2 \\ A_0^3 & A_1^3 & A_2^3 \\ A_0^4 & A_1^4 & A_2^4 \end{pmatrix} \begin{pmatrix} S_0^1 & \cdots & S_0^n \\ S_1^1 & \cdots & S_1^n \\ S_2^1 & \cdots & S_2^n \end{pmatrix}; \tag{8}$$

$$I_{cal} = \mathbf{A}S.$$

Then, the measurement matrix can be obtained by:

$$\mathbf{A} = I_{cal}\tilde{S}^{-1};\ \text{with}\ \tilde{S}^{-1} = S^T(SS^T)^{-1}. \tag{9}$$

Each row of the calibration matrix $\mathbf{A}$ corresponds to the analyzer of each sub-pixel. After the measurement matrix $\mathbf{A}$ is obtained, the incident polarization state $\boldsymbol{S}$ can be calculated by its pseudo-inverse matrix, $\mathbf{A}_{\boldsymbol{P}}{}^{\mathbf{-1}}$, called the polarization data reduction matrix.

$$S = \mathbf{A}_p^{-1} \cdot I;\ \text{with}\ \mathbf{A}_p^{-1} = (\mathbf{A}^T\mathbf{A})\mathbf{A}^T. \tag{10}$$

Where $\boldsymbol{I}$ is the measurement vector of each superpixel captured by CMOS. For linear polarization imaging, the degree of linear polarization ($DoLP$) and angle of polarization (AoP) can be calculated by solved Stokes vector $\boldsymbol{S}$, as shown in Eqs. (11)–(12).

$$DoLP = \sqrt{S_1^2 + S_2^2}/S_0; \tag{11}$$

$$AoP = \frac{1}{2}\arctan(S_2/S_1). \tag{12}$$

4.2. Polarization measurements

Firstly, the $DoLP$ and AoP of different linearly polarized light were measured. The polarizer was rotated from 0° to 180° at intervals of 10°. The results are shown in Fig. 10(a)-(b). Black

Optics EXPRESS

solid lines represent simulation values of *DoLP* and *AoP*. The circles and error bars represent the average measurements and standard deviations of all superpixels, respectively. The differences between the simulations and average measurements (errors) for *DoLP* and *AoP* are shown in Fig. 10(c) and (d). The results show that for each test wavelength, the error of *DoLP* for linearly polarized light is less than 1.15%. This indicates that the polarimeter system based on proposed twisted-LCMP has a high accuracy for *DoLP* measurement of linearly polarized light, which can meet the polarization detection requirements. The error of *AoP* is less than 0.65°. The reconstruction accuracy of *AoP* could be further improved if using super-pixel calibration method [31].

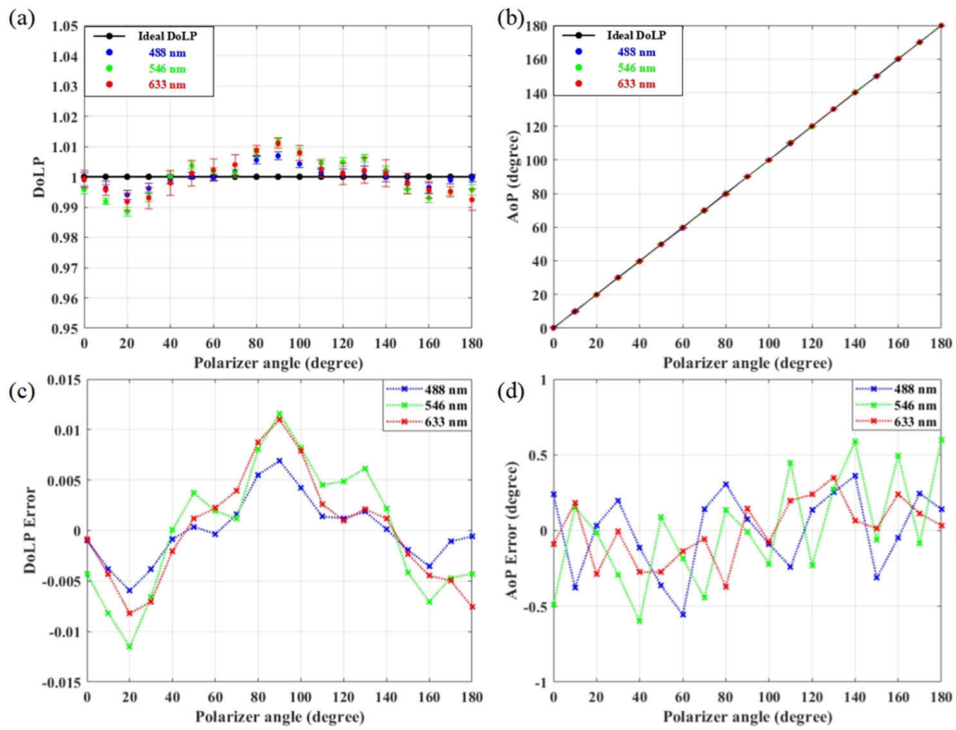

Fig. 10. (a) Degree of linear polarization (*DoLP*) and (b) angle of polarization (*AoP*) of monochromatic polarized light at 488 nm, 546 nm and) 633 nm were measured as a function of rotating a linear polarizer. The black solid lines represent simulated values. The circles and error bars respectively represent the mean measurements and standard deviations of all superpixels. (c) and (d) represent the difference between *DoLP* and *AoP* theoretical values and average measurements.

Serial of polarized light with different *DoLP* was generated by rotating an achromatic λ/4 retarder (AQWP10M-580, from Thorlabs) after a 0° polarizer. The retardances of the retarder were about 87.84° (@488 nm), 86.72° (@546 nm) and 87.05° (@633 nm). The retarder was rotated from 0° to 180° with a 10° increment. The results were shown in Fig. 11(a)-(c). The solid points and error bars represent the average value and standard deviation respectively of all superpixels. Solid lines represent theoretical simulation curves. Figure 11(d) illustrates the error of *DoLP* between measurement and simulation. The maximum errors of *DoLP* are about 7% (@ 488 nm), 2.5% (@ 546 nm) and 4.3% (@ 633 nm), respectively. The errors of the *DoLP* measurements are mainly attributed to the finite bandwidth of the bandpass filter and deviation of the retarder's retardances which cannot be removed by calibration. The standard deviations of *DoLP*, shown in Fig. 11(e) are less than 1.2% (@ 488 nm), 0.7% (@ 546 nm) and 0.8%

Optics EXPRESS

(@ 633 nm). The results show that the standard deviation of *DoLP* based on twisted-LCMP polarimeter is about 1%. For comparison, the average standard deviation of *DoLP* measured by the guest-host polymer LCMP polarimeter was about 5.31% [17]. The improvement in this work is mainly attributed to the higher extinction ratio of the twisted-LCMP which provides higher SNR. Meanwhile, the polarimeter system adopted in this paper greatly reduced the impact of misalignment and cross-talk on the measurement.

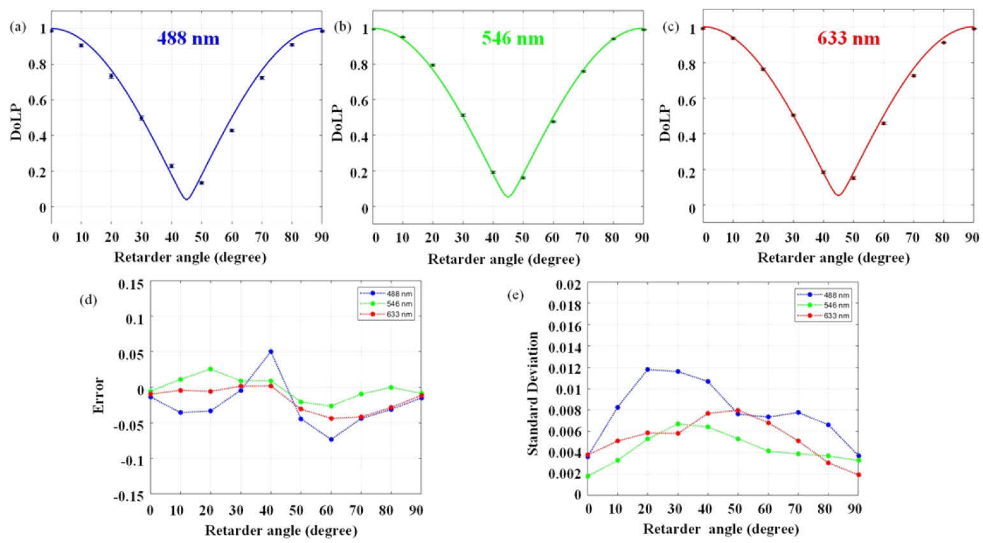

Fig. 11. The *DoLP* were measured as a function of the fast axis orientation of an achromatic λ/4 retarder at (a) 488 nm, (b) 546 nm and (c) 633 nm, respectively. The circles and the solid line presented the average of measurements and the simulated values. The error bars represented standard deviation in the *DoLP* of all superpixels. The error (d) and the standard deviation (e) of the *DoLP* were plotted as a function of retarder angles.

The remaining errors of the above *DoLP* and *AoP* measurements are mainly attributed to round off errors in intensity extraction and reconstruction calculation. Meanwhile, since the rotation of the polarizer and retarder were performed manually with an accuracy of about 0.5°, the accuracy of calibration as well as measurement are also affected by the orientation error of these rotating devices. These problems could be improved by improving the accuracy of the equipment.

4.3. Imaging experiments

A 0.32x double-telecentric lens (F/8) was placed in front of the twisted-LCMP array as an objective to perform imaging experiments. The test target was a perforated opaque aluminum sheet, as shown in the Fig. 12(a). Linear polarizers oriented differently were placed manually in each hole (4 mm×4 mm). And there was a 4 mm-diameter circular hole at the center without polarizer. The test target was illuminated by a 546 nm unpolarized light (a white LED combined with a 546 nm bandpass filter). Raw image captured by the camera are shown in the Fig. 12(b). *DoLP* and *AoP* pseudo-color images are shown in Fig. 12(c) and (d). Due to the intensity gradient around edges, the measured light flux will fluctuate and the data reduction will miscalculate and generate a polarization artifact [32]. Therefore, in the final results the data at the edge of each hole and the opaque part was removed. The average DoLP of the 8 polarizer regions is 0.994 ± 0.023. The AoP plot is uniform in polarizer region. The average *DoLP* of the circular hole in the middle is 0.021 ± 0.016 due to the unpolarized light directly passing through. The *AoP* plot is noisy in this region as expected, since there is no definite polarization axis for unpolarized light.

Optics EXPRESS

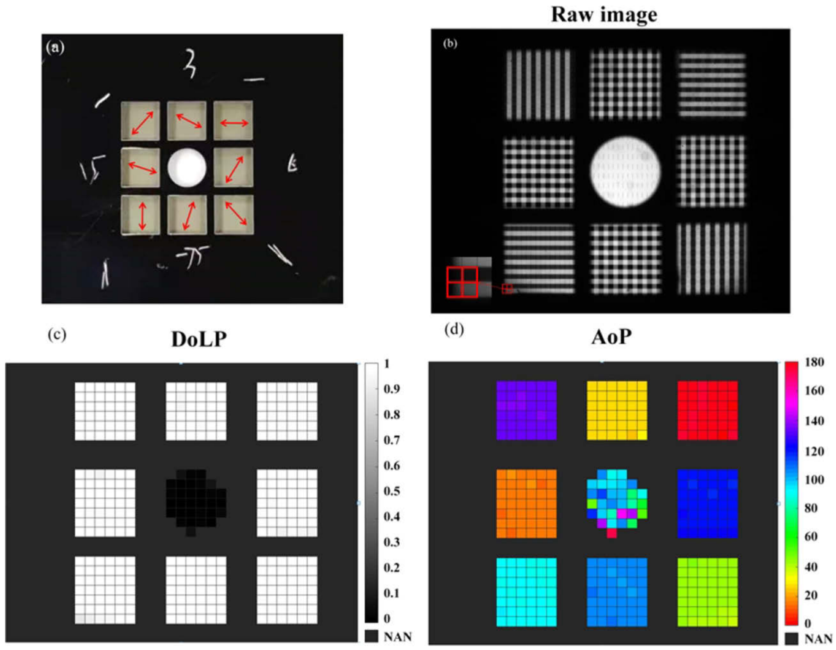

Fig. 12. (a) Photo of the test target. Eight polarizers were manually pasted into the square holes. Red arrows represented the general directions of the polarizers. (b) The test target was illuminated with a 546 nm unpolarized light source, and the raw image was captured by CMOS; A red square shows a superpixel on the edge. (c) DoLP and (d) AoP pseudo-color images of the target. The data at the edge of each hole and the opaque part were removed in the final results.

Then, the above-mentioned achromatic λ/4 phase retarder (86.72° retardance @ 546 nm) was inserted with a fast axis of 0° after the target. This approach simulated samples with different polarization characteristics. Figure 13 shows the raw image and the *DoLP* image. In the region where the polarizer orientation is near parallel or perpendicular to the fast axis of the retarder, the output light is near linearly polarized and *DoLP* is close to 1. When the angle between the polarizer orientation and the fast axis of the retarder is about 45° (or −45°), the output light is near-circularly polarized. For linearly polarimeter system, the circularly polarized light is indistinguishable from unpolarized light. Therefore, *DoLP* for the ±45° polarizer and non-polarizer regions are both close to 0.

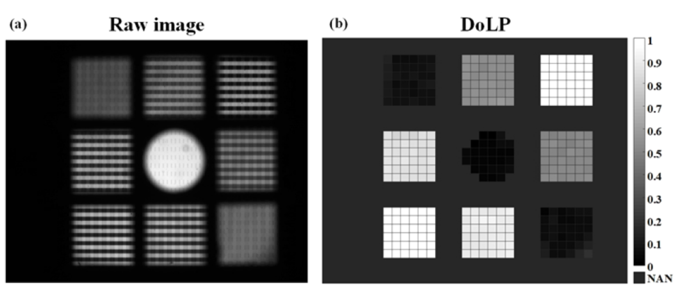

Fig. 13. The achromatic λ/4 phase retarder was inserted after the test target with a fast axis of 0°. (a) The raw image of the target. (b) *DoLP* image of the target.

5. Conclusion

In this paper, a 4 - domain micropolarizer array based on twisted-LC structure was designed and successfully fabricated for linear polarization imaging in the visible band. The proposed twisted-LCMP array was composed of a pixelated twisted-LC layer and a uniform film polarizer. To obtain the best extinction ratio, the twist angles in superpixels were optimized to be ±22.5° and ±67.5°, respectively. The twisted-LCMP array made by DMD lithography system is uniform with few defects and accurate twist angles. This method does not need aligned masks, and removes the requirement for any high-precision etching during the fabrication process of the micropolarizer array. Experimental results show that the extinction ratio of 22.5°-twisted LCMP is 6286, and that of 67.5°-twisted LCMP is about 1479 (@632.8 nm). A modular polarimeter system was built for polarization measurement and imaging experiments. The results show that the error of DoLP is less than 1.15% and that of AoP is less than 0.65° for linearly polarization input. For different degrees of linear polarization polarized inputs, the error of DoLP is less than 2.5% and the standard deviation is less than 0.7% (@546 nm). All the results indicate that the polarimeter system based on twisted-LCMP has high measurement accuracy and can meet the requirements of polarization detection.

Future work will focus on integrating the twisted-LCMP array on the top of an image sensor like CMOS and CCD to achieve a high-resolution, compact polarization camera. This will make the polarimeter more convenient to use, especially for outdoor scene. A feasible scheme is to place the polarizer directly on the sensor as the bottom substrate, and a micro-lenses array can be used as the top substrate. Turn on the sensor for pixel-to-pixel photoalignment, which could avoid the alignment error between LCMP and CMOS pixels. Besides, the measurement accuracy could be further improved by adopting the super-pixel calibration method. This work shows a promising and cost-effective solution compared to polarization cameras based on MWGP array.

Funding. National Natural Science Foundation of China (11604327, 11974345, 61775212, 61875036, 61975202, U2030101); Chinese Academy of Sciences President's International Fellowship Initiative (2020VTA0004); Jilin Scientific and Technological Development Program (20190302049GX).

Disclosures. The authors declare no conflicts of interest.

Data availability. Data underlying the results presented in this paper are not publicly available at this time but may be obtained from the authors upon reasonable request.

References

1. G. C. Giakos, "Multifusion, Multispectral, Optical Polarimetric Imaging Sensing Principles," IEEE Trans. Instrum. Meas. **55**(5), 1628–1633 (2006).
2. J. S. Tyo, M. P. Rowe, E. N. Pugh Jr., and N. Engheta, "Target detection in optically scattering media by polarization-difference imaging," Appl. Opt. **35**(11), 1855–1870 (1996).
3. M. Novak, J. Millerd, N. Brock, M. North-Morris, J. Hayes, and J. Wyant, "Analysis of a micropolarizer array-based simultaneous phase-shifting interferometer," Appl. Opt. **44**(32), 6861–6868 (2005).
4. N. Brock, B. Kimbrough, and J. Millerd, "A pixelated polarizer-based camera for instantaneous interferometric measurements," Proc. SPIE **8160**, 81600W (2011).
5. M. Garcia, C. Edmiston, R. Marinov, A. Vail, and V. Gruev, "Bio-inspired color-polarization imager for real-time in situ imaging," Optica **4**(10), 1263–1271 (2017).
6. J. Qi, C. He, and D. S. Elson, "Real time complete Stokes polarimetric imager based on a linear polarizer array camera for tissue polarimetric imaging," Biomed. Opt. Express **8**(11), 4933–4946 (2017).
7. J. S. Tyo, D. L. Goldstein, D. B. Chenault, and J. A. Shaw, "Review of passive imaging polarimetry for remote sensing applications," Appl. Opt. **45**(22), 5453–5469 (2006).
8. N. Gu, B. Yao, L. Huang, and C. Rao, "Design and Analysis of a Novel Compact and Simultaneous Polarimeter for Complete Stokes Polarization Imaging with a Piece of Encoded Birefringent Crystal and a Micropolarizer Array," IEEE Photonics J. **10**(2), 1–12 (2018).
9. M. Kulkarni and V. Gruev, "Integrated spectral-polarization imaging sensor with aluminum nanowire polarization filters," Opt. Express **20**(21), 22997–23012 (2012).
10. Z. Zhang, F. Dong, T. Cheng, K. Qiu, Q. Zhang, W. Chu, and X. Wu, "Nano-fabricated pixelated micropolarizer array for visible imaging polarimetry," Rev. Sci. Instrum. **85**(10), 105002 (2014).
11. J. Guo and D. Brady, "Fabrication of thin-film micropolarizer arrays for visible imaging polarimetry," Appl. Opt. **39**(10), 1486–1492 (2000).

12. V. Gruev, A. Ortu, N. Lazarus, J. V. Spiegel, and N. Engheta, "Fabrication of a dual-tier thin film micropolarization array," Opt. Express **15**(8), 4994–5007 (2007).
13. X. Zhao, A. Bermak, F. Boussaid, T. Du, and V. G. Chigrinov, "High-resolution photoaligned liquid-crystal micropolarizer array for polarization imaging in visible spectrum," Opt. Lett. **34**(23), 3619–3621 (2009).
14. X. Zhao, A. Bermak, F. Boussaid, and V. G. Chigrinov, "Liquid-crystal micropolarimeter array for full Stokes polarization imaging in visible spectrum," Opt. Express **18**(17), 17776–17787 (2010).
15. G. Myhre, A. Sayyad, and S. Pau, "Patterned color liquid crystal polymer polarizers," Opt. Express **18**(26), 27777–27786 (2010).
16. X. Zhao, F. Boussaid, A. Bermak, and V. G. Chigrinov, "High-resolution thin "guest-host" micropolarizer arrays for visible imaging polarimetry," Opt. Express **19**(6), 5565–5573 (2011).
17. G. Myhre, W.-L. Hsu, A. Peinado, C. LaCasse, N. Brock, R. A. Chipman, and S. Pau, "Liquid crystal polymer full-stokes division of focal plane polarimeter," Opt. Express **20**(25), 27393–27409 (2012).
18. W.-L. Hsu, G. Myhre, K. Balakrishnan, N. Brock, M. Ibn-Elhaj, and S. Pau, "Full-Stokes imaging polarimeter using an array of elliptical polarizer," Opt. Express **22**(3), 3063–3074 (2014).
19. W.-L. Hsu, K. Balakrishnan, I.-E. Mohammed, and S. Pau, "Infrared liquid crystal polymer micropolarizer," Appl. Opt. **53**(23), 5252–5258 (2014).
20. V. G. Chigrinov, *Liquid Crystal Photonics*, (Nova Science Publisher, 2014), Chap. 4.
21. P. Yeh and C. Gu, *Optics of Liquid Crystal Displays*, 2nd Edition (John Wiley & Sons, 2009), Chap. 4.
22. J. S. Tyo, "Design of optimal polarimeters: maximization of signal-to-noise ratio and minimization of systematic error," Appl. Opt. **41**(4), 619–630 (2002).
23. Z. Peng, Z. Cao, L. Yao, Q. Mu, Y. Liu, Q. Wang, D. Li, and L. Xuan, "The review of liquid crystal wavefront corrector with fast response property (in Chinese)," Sci. Sin-Phys. Mech. Astron. **47**(8), 084203 (2017).
24. L. Xuan, Z. Peng, Y. Liu, L. Yao, L. Hu, Z. Chao, Q. Mu, D. Li, M. Xia, C. Yang, and X. Lu, "The preparation method of liquid crystal materials used in the liquid crystal wavefront corrector (in Chinese)," PRC Patent, CN201210046752.2, (2013).
25. S. Gauza, J. Li, S.-T. Wu, A. Spadlo, R. Dabrowski, Y.-N. Tzeng, and K.-L. Cheng, "High birefringence and high resistivity isothiocyanate-based nematic liquid crystal mixtures," Liq. Cryst. **32**(8), 1077–1085 (2005).
26. M.-C. Tseng, O. Yaroshchuk, T. Bidna, A. K. Srivastava, V. Chigrinov, and H.-S. Kwok, "Strengthening of liquid crystal photoalignment on azo dye films: passivation by reactive mesogens," RSC Adv. **6**(53), 48181–48188 (2016).
27. Y. Zhang, J. Luo, Z. Xiong, H. Liu, L. Wang, Y. Gu, Z. Lu, J. Li, and J. Huang, "User-defined microstructures array fabricated by dmd based multistep lithography with dose modulation," Opt. Express **27**(22), 31956–31966 (2019).
28. S. Guo, Z. Lu, Z. Xiong, L. Huang, H. Liu, and J. Li, "Lithographic pattern quality enhancement of DMD lithography with spatiotemporal modulated technology," Opt. Lett. **46**(6), 1377–1380 (2021).
29. V. Chigrinov, H. S. Kwok, H. Takada, and H. Takatsu, "Photo-aligning by azo-dyes: physics and applications," Liq. Cryst. Today **14**(4), 1–15 (2005).
30. A. Lizana, J. Campos, A. V. Eeckhout, and A. Marquez, "Misalignment error analysis in polychromatic division of focal plane stokes polarimeters," OSA Continuum **2**(5), 1565–1575 (2019).
31. S. B. Powell and V. Gruev, "Calibration methods for division-of-focal-plane polarimeters," Opt. Express **21**(18), 21039–21055 (2013).
32. R. A. Chipman, W. -S. T. Lam, and G. Young, *Polarized Light and Optical Systems* (Chemical Rubber Company, 2018), Chap. 7.